Palaeogeography, Palaeoclimatology, Palaeoecology 615 (2023) 111437

Contents lists available at ScienceDirect

Palaeogeography, Palaeoclimatology, Palaeoecology

journal homepage: www.elsevier.com/locate/palaeo

Karst-ecological changes during the middle and late Holocene in Southwest China revealed by $\delta^{18}O$ and $\delta^{13}C$ records in a stalagmite

Rong Duan [a], Ting-Yong Li [a,*], Jun-Yun Li [b,**], Christoph Spötl [c], Hong-Chun Li [d], Hai-Bo Wang [e], Hai Cheng [e], You-Feng Ning [e], Chuan-Chou Shen [f,g], Jing-Li Zhou [b], Chao-Jun Chen [a,b], Tsai-Luen Yu [f,g,h], R. Lawrence Edwards [i], Zi-Qi Liu [j]

[a] Yunnan Key Laboratory of Plateau Geographical Processes & Environmental Changes, Faculty of Geography, Yunnan Normal University, Kunming 650500, China
[b] Chongqing Key Laboratory of Karst Environment, School of Geographical Sciences; Southwest University, Chongqing 400715, China
[c] Institute of Geology, University of Innsbruck, Innrain 52, 6020 Innsbruck, Austria
[d] Department of Geosciences, National Taiwan University, Taipei 10617, Taiwan
[e] Institute of Global Environmental Change, Xi'an Jiaotong University, Xi'an 710049, China
[f] High-precision Mass Spectrometry and Environment Change Laboratory (HISPEC), Department of Geosciences, National Taiwan University, Taipei 10617, Taiwan
[g] Research Center for Future Earth, National Taiwan University, Taipei 10617, Taiwan
[h] Marine Industry and Engineer Research Center, National Academy of Marine Research, Kaohsiung 806614, Taiwan
[i] Department of Earth and Environmental Sciences, University of Minnesota, Minneapolis, MN, USA
[j] School of Karst Science, Guizhou Normal University, Guiyang 550001, China

ARTICLE INFO

Editor: P. Hesse

Keywords:
Middle and late Holocene
Speleothems
Asian summer monsoon
Karst
Societal changes

ABSTRACT

Rocky desertification is a major environmental problem in the karst regions of Southwest China and seriously impacts ecological and socioeconomic development. Human activities and climate change have been proposed as the main factors responsible for the development and expansion of rocky desertification, but more evidence is needed to support this hypothesis. In this study, the history of the Asian summer monsoon (ASM) since 6200 yr BP is reconstructed based on ^{230}Th dating and $\delta^{18}O$ and $\delta^{13}C$ data of a stalagmite from Feilong Cave in Guizhou Province of Southwest China. Positive $\delta^{18}O$ and $\delta^{13}C$ excursions record eleven interdecadal–centennial weak summer monsoon events at 1000–870, 1660–1460, 2040–1900, 2780–2460, 3020–2860, 3250–3120, 3650–3370, 4273–3980, 4820–4480, 5370–5180, and 5840–5560 yr BP. These weak ASM events were controlled by a southward shift of the Intertropical Convergence Zone and frequent El Niño events. Changes in the $\delta^{13}C$ values of this stalagmite were mainly driven by changes in vegetation coverage and type, soil microbial activity, and regional hydrogeological conditions. The simultaneous positive excursions of $\delta^{18}O$ and $\delta^{13}C$ at ~5500, 4200, and 2800 yr BP indicate a degradation of the karst ecological environment in response to the weak summer monsoon. In addition, frequent dynasty changes in China since 3000 yr BP profoundly influenced the karst ecological environment. During the Medieval Warm Period, the Jing-Kang event (JK event) resulted in the fall of the Northern Song Dynasty and led to a large-scale migration into southern China. As a consequence, the population increase in the Yangtze River basin enhanced land use, accelerated the disappearance of forests, and finally resulted in the deterioration of the regional environment. We conclude that climate change and anthropogenic activity may have jointly triggered and/or exacerbated rocky desertification in Southwest China.

1. Introduction

The karst regions of Southwest China cover an area of 7.5×10^5 km^2, accounting for 43% of the total area of Southwest China (Zeng et al., 2016). This area is deeply influenced by the Indian summer monsoon (ISM) and the East Asian summer monsoon (EASM) and is highly sensitive to global climate change (Li et al., 2012a). Guizhou Province is the center of karst in Southwest China. Historical data from 1900 to 2012 CE

* Corresponding author at: Yunan Key Laboratory of Plateau Geographical Processes & Environmental Changes, Faculty of Geography, Yunnan Normal University, Kunming 6505500, China.
** Corresponding author at: Chongqing Key Laboratory of Karst Environment, School of Geographical Sciences; Southwest University, Chongqing 400715, China.
E-mail addresses: cdlity@163.com (T.-Y. Li), jxljy@swu.edu.cn (J.-Y. Li).

https://doi.org/10.1016/j.palaeo.2023.111437
Received 13 September 2022; Received in revised form 12 January 2023; Accepted 1 February 2023
Available online 4 February 2023
0031-0182/

showed that droughts and floods occurred frequently (198 times) in the karst areas of Southwest China, especially in Guizhou Province (Guo et al., 2015; Li et al., 2012b; Cheng et al., 2020). Therefore, exploring the history of changes in climate and the karst ecological environment in this region is important for studying the interaction between human activities and the environment (Chen et al., 2021b).

On the orbital time scale, insolation controls long-term variations in the Asian summer monsoon (ASM) (Cheng et al., 2016; Wang et al., 2017; Wu et al., 2020). However, internal feedbacks (El Niño–Southern Oscillation (ENSO), Atlantic Meridional Overturning Circulation (AMCO), shifts of the Intertropical Convergence Zone (ITCZ) and volcanic activity) in the climate system are invoked for changes in the ASM on shorter time scales (Wan et al., 2011; Zhao et al., 2017; Zhang et al., 2017; Cheng et al., 2019; Li et al., 2021a,b; Chen et al., 2021a). In recent decades, many achievements have been made in the study of climate change in the Asian monsoon region by using lacustrine sediments, tree rings and historical documents (Wang et al., 2005; Xiao et al., 2014; Duan et al., 2014). However, understanding the evolution of the ASM on interdecadal–centennial time scales still needs further study (Tan, 2016). Stalagmites from caves in the ASM region are a key archive to address these questions, given their high resolution, excellent chronology and the availability of multiple climate and environmental proxies (Cheng et al., 2012, 2019).

In addition, the transport processes and mechanisms of carbon isotopes in karst systems have been studied in recent years (Liu et al., 2008; Zhang et al., 2015a,b; Liu et al., 2016; Li et al., 2018; Li and Li, 2018). The $\delta^{13}C$ values of stalagmites are affected by climatic and nonclimatic factors (Li et al., 2018). Nonclimatic factors include the connectivity of bedrock fissures, prior calcite precipitation, time of interaction between water and bedrock, ventilation in caves, and isotopic fractionation during carbonate deposition (Spötl et al., 2005; Fairchild et al., 2006; Liu et al., 2016; Li et al., 2018). On the interdecadal–centennial scale, the $\delta^{13}C$ values of stalagmites are mainly controlled by regional environmental changes outside the cave, such as changes in vegetation coverage, soil microbial activities, and the regional hydrological cycle (Baker et al., 1997; Fairchild et al., 2006; Zhang et al., 2015a,b; Liu et al., 2016; Li and Li, 2018). Rocky desertification is a main environmental problem in karst areas, and is characterized by serious soil erosion, missing surface water, loss of vegetation and exposed rocks (Jiang et al., 2016). The $\delta^{13}C$ values of stalagmites can be used as a proxy for the reconstruction of the paleoenvironment; and to study the evolution of rocky desertification in karst areas (Li et al., 2012a; Oster et al., 2012; Chen et al., 2021a, 2021b). The comparison of stalagmite $\delta^{18}O$ and $\delta^{13}C$ values is very important in reconstructing climate change in the karst areas of Southwest China, exploring the interaction between humans and the environment, and assessing the impact of climate change. Recent research suggests that the expansion of karst rocky desertification in southwestern China was exacerbated in the MWP due to the change in climate, wars, and rises and falls of dynasties, which resulted in the migration of a large number of people and large-scale reclamation of arable land (Yassoglou, 2000; Liu et al., 2011; Kuo et al., 2011; Chen et al., 2021b). During the MWP, wars occurred in northern China for many years, resulting in a sharp decrease in the total population and the migration of a large number of people from northern to southern China (Wu, 2000; Zhang and Peng, 2012). Massive immigration not only brought advanced production technology and C4 plant crops to southern China, but also required the reclamation of a great deal of land and slope cropland, and the enhancement of agricultural production and rural infrastructure (Zhang and Peng, 2012; Fang et al., 2015). In the meantime, the massive deforestation caused by population migration (Zhao et al., 2015), resulted in the reduction of vegetation coverage (Kuo et al., 2011), serious soil erosion and deterioration of surface hydrologic conditions, and finally presented karst rocky desertification (Liu et al., 2011; Kuo et al., 2011). However, more evidence is needed to confirm whether this phenomenon is local or regional in scale. Herein, we report a $\delta^{18}O$ record of a ^{230}Th-dated stalagmite from Feilong Cave, Southwest China (SW-China), which we compare with other records to assess climate changes across Southwest China regions during the middle late Holocene. This study focuses on the following issues: (1) How the evolution of the ASM in the middle late Holocene affected the karst environment in southwestern China on the interdecadal- centennial scale. (2) Changes in the karst environment in Southwest China during the middle and late Holocene, and (3) stalagmite $\delta^{13}C$ records in Southwest China were used to explore the influence of human activities and climate change on karst rocky desertification.

2. Settings

Feilong (FL) Cave (24°58′13″N, 104°52′54″E) is located in Guizhou Province, Southwest China (Fig. 1). It is located in the gradual slope of the eastern part of the Yunnan-Guizhou Plateau, and developed in Triassic dolomitic limestone. The natural entrance of the cave is 8 m high and 28 m wide, and the entire length of the cave is approximately 1000 m (Liu et al., 2008; Guo et al., 2006). The landscape of the area surrounding the cave is characterized by hilly topography as a peak cluster-depression, and the elevation is 1357 m for the entrance of the cave. The rock above the cave is approximately 60 m thick, and shrub vegetation grows on the surface (Fig. 2). FL Cave is located in an area strongly affected by the ASM, and the moisture during the rainy season mainly comes from the Indian and Pacific Oceans (Fig. 1). The region has an annual mean temperature of 16.1 °C and receives 1532 mm of annual precipitation, 80% of which falls between May and October. Hence, the study area features a subtropical monsoon climate (Liu et al., 2008) (Supplementary Fig. 1). The karst area covers an area of 1.2×10^5 km^2 in Guizhou Province, and 68% of its surface consists of karst landforms (Jiang et al., 2016).

3. Sample and methods

Stalagmite FL2 is a broken stalagmite composed of three sections, with a diameter of approximately 84 mm at the bottom and approximately 65 mm at the top. The total length measured along its growth axis is 430 mm (Fig. 3). With the use of a dental drill with a diameter of 1 mm, 7 powder samples (50–100 mg each) were drilled along the growth axis for ^{230}Th dating. U and Th were separated using standard chemical procedures described by Edwards et al. (1987), Shen et al. (2012), and Cheng et al. (2013). ^{230}Th dating was performed in the Isotope Laboratory of the Institute of Global Environmental Change of Xi'an Jiaotong University using a multicollector inductively coupled plasma mass spectrometer (MC–ICP–MS). The uncertainties in the U-Th isotopic data were calculated offline at the 2σ level (Cheng et al., 2016). The decay constant used for ^{230}Th was 9.1705×10^{-6} yr^{-1} (Cheng et al., 2013), that used for ^{234}U was 2.82206×10^{-6} yr^{-1} (Cheng et al., 2013), and that used for ^{238}U was 1.55125×10^{-10} yr^{-1} (Jaffey et al., 1971). An initial ^{230}Th/^{232}Th atomic ratio of $(4.4 \pm 2.2) \times 10^{-6}$ was assumed for the correction of the ^{230}Th ages. These are the values for materials in secular equilibrium with the bulk Earth ^{232}Th/^{238}U value.

With a dental drill, a total of 410 samples were collected from the polished profile along the central growth axis of the stalagmite for isotopic analysis. The samples were drilled at intervals of ~1 mm. The $\delta^{18}O$ and $\delta^{13}C$ analyses of stalagmite FL2 were performed using the Delta V Plus isotope ratio mass spectrometer at the Institute of Geology, University of Innsbruck, Austria. The results are reported relative to the Vienna Pee Dee Belemnite (V-PDB) standard. The analytical error is <0.08‰ for $\delta^{18}O$ and <0.06‰ for $\delta^{13}C$ (Spötl and Vennemann, 2003).

To assess the possibility of calcite deposition under isotopic equilibrium conditions (the Hendy test) (Hendy, 1971), ten layers along the growth axis of stalagmite FL2 were chosen with which to analyze the stable oxygen and carbon isotopes. For each layer, from the center of the growth axis to the edge, six or seven subsamples were drilled and analyzed as described above for isotopic analysis.

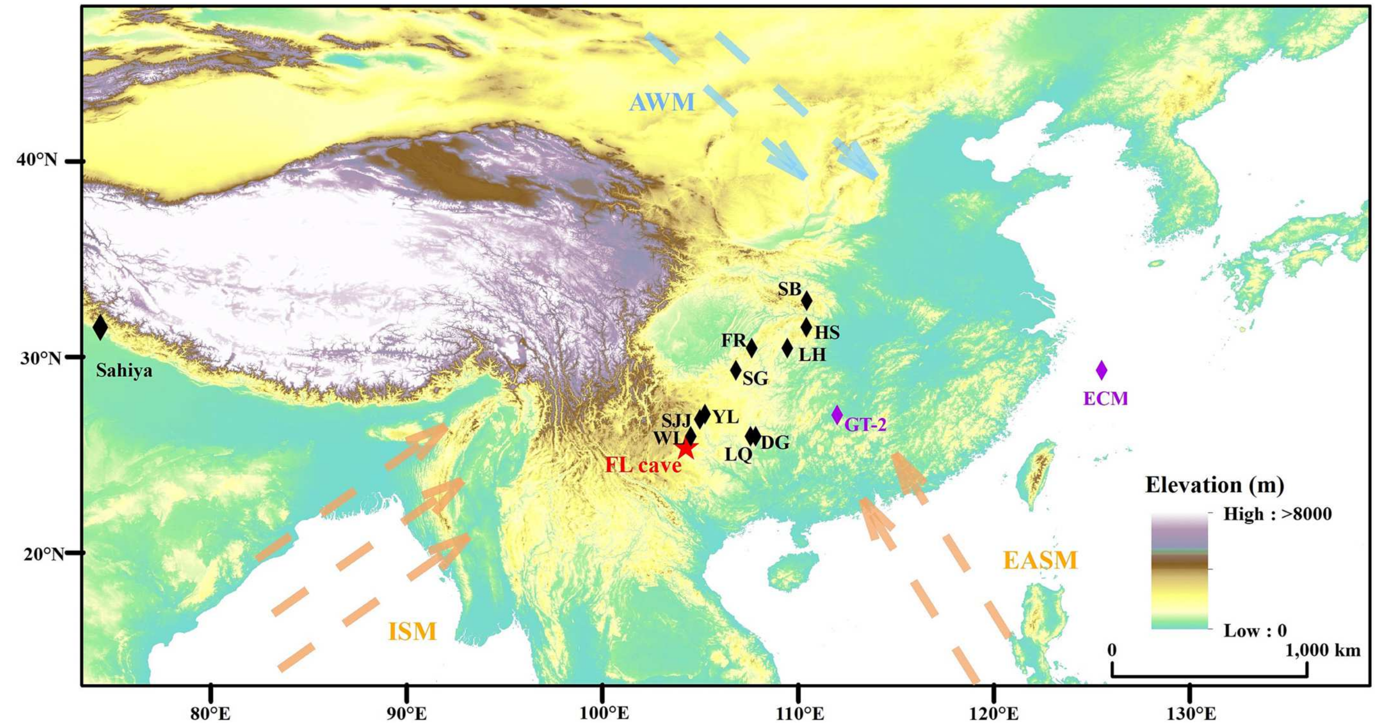

Fig. 1. Location of Feilong (FL) Cave in Southwest China. The red star indicates the location of FL Cave (this study); the black diamonds indicate Sahiya Cave (Kathayat et al., 2017), Dongge Cave (DG) (Wang et al., 2005), Longquan Cave (LQ) (Zhang et al., 2004), Shijiangjun Cave (SJJ) (Chen et al., 2021a, 2021b), Wulu Cave (WL) (Mohtadi et al., 2016), Yelang Cave (YL) (M. Zhao et al., 2017), Shigao Cave (SG) (Jiang et al., 2012), Furong Cave (FR) (Li et al., 2021a), Lianhua Cave (LH) (Zhang et al., 2013), Heshang Cave (HS) (Hu et al., 2008), and Sanbao Cave (SB) (Dong et al., 2010). The dashed orange arrows represent the surface wind directions of the ISM and the EASM, and the blue arrows represent the surface wind direction of the Asian winter monsoon (AWM). The purple diamond represents the site of core GT-2, from which microcharcoal was extracted (Ma et al., 2018), and core ECMS, from which black carbon was extracted (Pei et al., 2020). (For interpretation of the references to colour in this figure legend, the reader is referred to the web version of this article.)

4. Results

The ^{230}Th dating results for stalagmite FL2 are presented in Table 1. The ^{238}U contents of most of the samples range from 143 to 219 ppb, and the ^{232}Th contents of most of the dated samples range from 1347 to 5920 ppt. The low ^{230}Th/^{232}Th ratios (17–84 × 10^{-6}) give rise to relatively large age errors, with an average of ±244 yr. Because of the relatively low precision of the dating results (Table 1), we did not use the linear interpolation method to establish the age model. The Mod-Age model supports to calculating the relationship between age and depth at any position of the proxy-time profile and attempts to base all ages on a single time series (Hercman and Pawlak, 2012), different from the StalAge model (Scholz and Hoffmann, 2011). Therefore, the Mod-Age model was finally used to build the chronology of the FL2 record. The results show that stalagmite FL2 grew between 6290 and 690 yr BP (Fig. 3B).

The δ^{18}O values of stalagmite FL2 range from −8.2‰ to −5.5‰, with a mean of −7.0‰. During 690–6290 yr BP, the δ^{18}O values exhibit an overall positive trend (Fig. 4). In addition, at 870–1000, 1460–1660, 1900–2040, 2460–2780, 2860–3020, 3120–3250, 3370–3650, 3980–4273, 4480–4820, 5180–5370, and 5560–5840 yr BP, the δ^{18}O values show offsets with amplitudes of 0.5–1‰ and are labeled events 1–11 (Fig. 4). The duration of these events is 130–340 years.

The δ^{13}C values of stalagmite FL2 range from −13.4‰ to −8.6‰, with a mean value of −11.7‰ (Fig. 4). Changes in the δ^{13}C and δ^{18}O values of stalagmite FL2 are positively correlated ($r = 0.62$; $p < 0.01$; $n = 410$) and both isotope values show positive excursions during the 11 events mentioned above (Fig. 4).

The results of the Hendy test are plotted in Supplementary Fig. 3. The range for the variability of δ^{18}O values in a coetaneous-layer was 0.52–1.02‰, and there was an apparent correlation between the δ^{18}O and δ^{13}C values for most of the layers (9/10). These observations suggested that the deposition of stalagmite FL2 did not satisfy the Hendy test. However, there are some limitations of the Hendy test criteria in judging the paleoclimatic suitability of speleothems, and the replication principle of comparing overlapping δ^{18}O profiles has been proven to be an effective method for assessing the suitability of speleothems in paleoclimatic reconstruction (Dorale and Liu, 2009). The δ^{18}O patterns of the FL2 and other stalagmites in monsoon China are agree within age uncertainties (in section 4), indicating that the FL2 record also satisfied the replication test. Therefore, we are confident that the variation in FL2 δ^{18}O is mainly dominated by climate change.

5. Discussion

5.1. *Significance of the stalagmite δ^{18}O values*

Many stalagmite δ^{18}O records in the ASM region have been used to demonstrate the intensity variation of the summer monsoon (Wang et al., 2001, 2005; Cosford et al., 2008; Cheng et al., 2016; Kathayat et al., 2017). For example, the δ^{18}O of a stalagmite from Dongge Cave reflected the intensity of the ASM on a centennial-millennial scale (Wang et al., 2005; Duan et al., 2014). Model simulation results have also shown that the δ^{18}O of stalagmites in the Asian monsoon region reflected the monsoon intensity (Liu et al., 2016). That is, the stronger the ASM is, the more negative the δ^{18}O of the stalagmite, and vice versa (Wang et al., 2005; Duan et al., 2014; Cheng et al., 2016, 2019). Comprehensive studies have shown that on the interdecadal–centennial scale, the δ^{18}O values of stalagmites from the East Asian monsoon region are affected by several factors, such as summer monsoon intensity, summer rainfall amount, moisture sources, rainout effects, and convective activities over the primary moisture source regions (Dayem

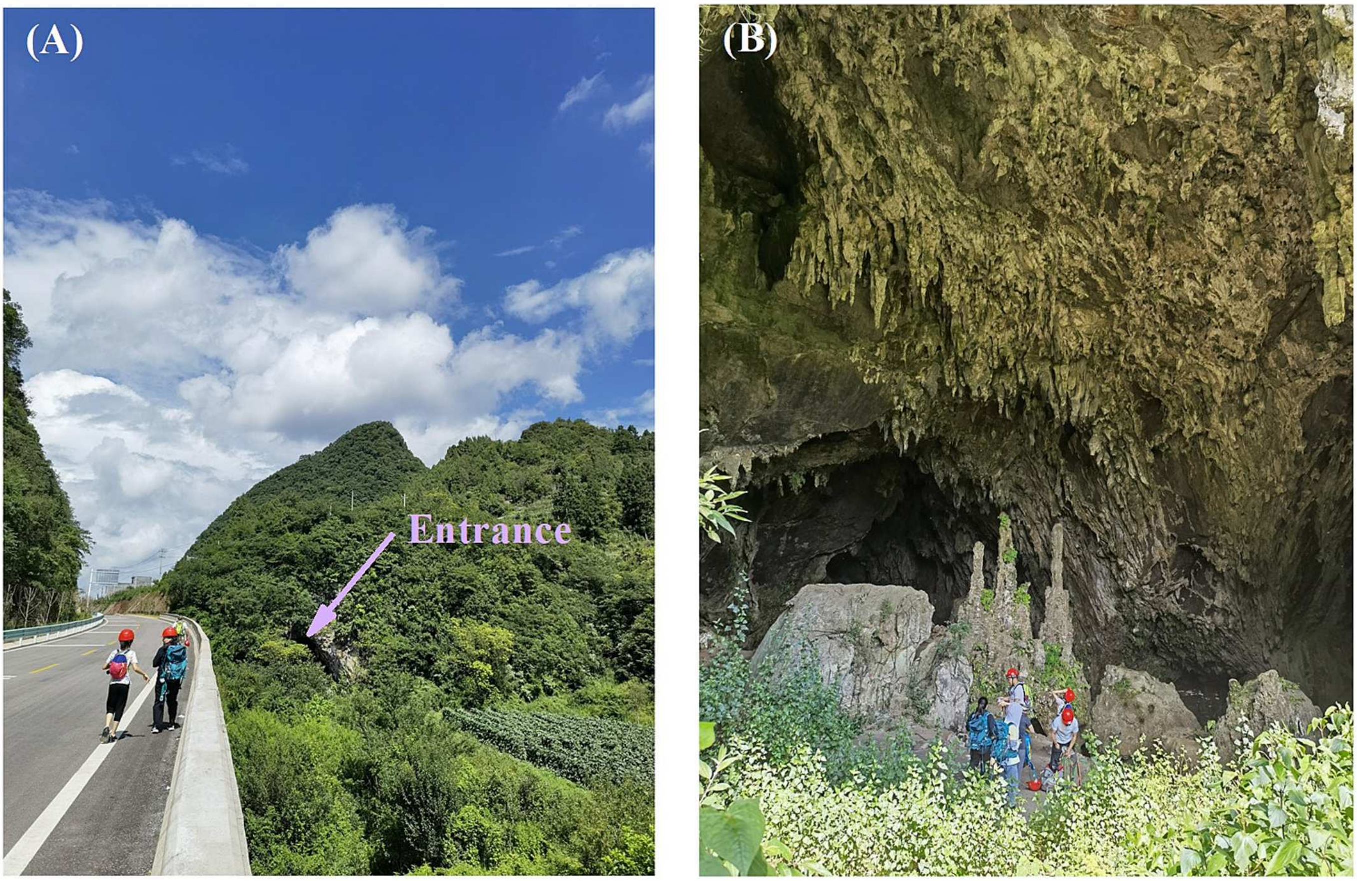

Fig. 2. (A) Local landscape and vegetation outside Feilong Cave. (B) Entrance of the cave.

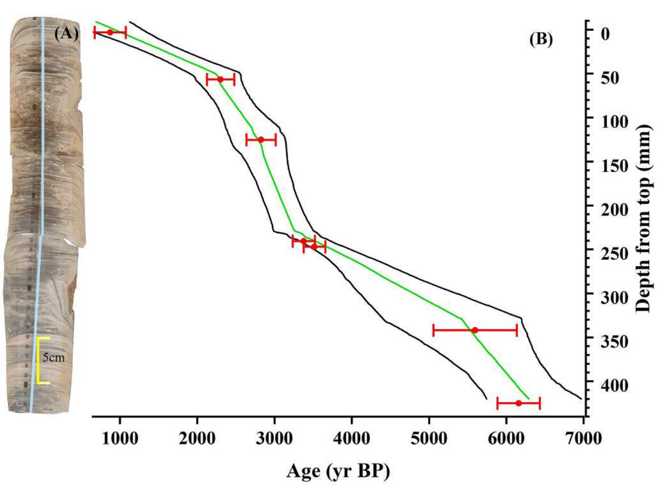

Fig. 3. (A) Cut section of stalagmite FL2. The cyan vertical bars show the path of stable isotope sampling. (B) Age model. The green solid line was obtained using MOD-AGE (Hercman and Pawlak, 2012), the black solid line represents the 98% confidence band, and the red error bars represent the dating points and the error ranges. (For interpretation of the references to colour in this figure legend, the reader is referred to the web version of this article.)

et al., 2010; Tan, 2014; Li, 2018a, 2018b; Ruan et al., 2019). Although on the interdecadal-centennial scale, the $\delta^{18}O$ values of stalagmites from Shenqi Cave have been used to reconstruct changes in rainfall in southwestern China (Tan et al., 2018), the $\delta^{18}O$ values of stalagmites are the cumulative changes in the entire process of water vapor migration from the vapor source to the cave location. Based on monitoring works in Southwest China, there was no negative correlation between summer precipitation and $\delta^{18}O$ of rainwater (Li, 2018a, 2018b). Therefore, Li et al. (2018) proposed that the changes in moisture source were the main reason for the seasonal and annual changes in precipitation $\delta^{18}O$, but not local precipitation. Modern observations at the Guiyang meteorological station 330 km from FL Cave during the period of 1988–1992 (A.D.) also indicated that the $\delta^{18}O$ values of summer monsoon precipitation were more negative than those of nonsummer monsoon precipitation. For example, the $\delta^{18}O$ values of summer (June, July, and August: JJA) range from −10.5‰ to −16.8‰, and the $\delta^{18}O$ values of nonsummer range from −8.5‰ to −0.6‰ (Liu et al., 2008) (Supplementary Fig. 1). Summer precipitation accounts for approximately 80% of the annual precipitation amount, demonstrating the significance of the ASM.

In addition, meteorological data (Zhang, 2020), climate modeling (Pausata et al., 2011), and paleoclimate records (Rehfeld et al., 2013) showed that in the ISM region, precipitation was dominated by moisture sources from the Indian Ocean, including the Bay of Bengal (Zhang et al., 2022). Precipitation $\delta^{18}O$ in Southwest China reflects not only changes in summer monsoon intensity, but also changes in the ratio of water vapor from the Indian Ocean and the Pacific Ocean (Tan, 2009, 2014; Zhang et al., 2022). In summary, although there are many factors influencing the change in precipitation (stalagmite) $\delta^{18}O$, at the first order, when the ASM was stronger, the $\delta^{18}O$ of stalagmite FL2 was more negative. In contrast, when the ASM was weaker, the $\delta^{18}O$ was more positive. For the change in local absolute precipitation and hydrological conditions, comprehensive analysis should be combined with other proxies, including $\delta^{13}C$ and trace elements (Chen et al., 2021a, 2021b; Wu et al., 2020, 2023).

Table 1
^{230}Th dating results for stalagmite FL2 from Feilong Cave in Guizhou province, China.

Sample Number	^{238}U (ppb)		^{232}Th (ppt)		^{230}Th / ^{232}Th (atomic x10^{-6})		δ^{234}U* (measured)		^{230}Th / ^{238}U (activity)		^{230}Th Age (yr) (uncorrected)		^{230}Th Age (yr) (corrected)		δ^{234}U$_{Initial}$** (corrected)		^{230}Th Age (yr BP) *** (corrected)	
FL2A-1	219.3	±0.2	2887	±58	17	±1	375.5	±1.4	0.0135	±0.0007	1077	±60	799	±206	376	±1	728	±206
FL2A-2	163.2	±0.1	1828	±37	45	±1	334.5	±1.5	0.0304	±0.0006	2507	±54	2263	±181	337	±2	2192	±181
FL2A-3	192.9	±0.1	2274	±46	50	±1	297.3	±1.4	0.0360	±0.0006	3062	±52	2797	±194	300	±1	2726	±194
FL2B-4	168.7	±0.1	1480	±30	81	±2	348.9	±1.4	0.0433	±0.0007	3552	±61	3364	±147	352	±1	3293	±147
FL2C-5	149.8	±0.1	1347	±27	84	±2	380.0	±1.6	0.0461	±0.0007	3696	±53	3507	±144	384	±2	3436	±144
FL2C-6	157.4	±0.1	5920	±119	35	±1	403.9	±1.8	0.0804	±0.0006	6413	±52	5635	±553	410	±2	5564	±553
FL2C-7	143.7	±0.1	2808	±56	73	±2	465.2	±1.7	0.0863	±0.0009	6598	±70	6212	±282	473	±2	6141	±282

U decay constants: $\lambda_{238} = 1.55125 \times 10^{-10}$ (Jaffey et al., 1971) and $\lambda_{234} = 2.82206 \times 10^{-6}$ (Cheng et al., 2013). Th decay constant: $\lambda_{230} = 9.1705 \times 10^{-6}$ (Cheng et al., 2013). *$\delta^{234}U = ([^{234}U/^{238}U]_{activity} - 1) \times 1000$. ** $\delta^{234}U_{initial}$ was calculated based on ^{230}Th age (T), i.e. , $\delta^{234}U_{initial} = \delta^{234}U_{measured} \times e^{\lambda 234 \times T}$. Corrected ^{230}Th ages assume the initial $^{230}Th/^{232}Th$ atomic ratio of $4.4 \pm 2.2 \times 10^{-6}$. Those are the values for a material at secular equilibrium, with the bulk earth $^{232}Th/^{238}U$ value of 3.8. The errors are arbitrarily assumed to be 50%. ***BP stands for "Before Present" where the "Present" is defined as the year 1950 CE.

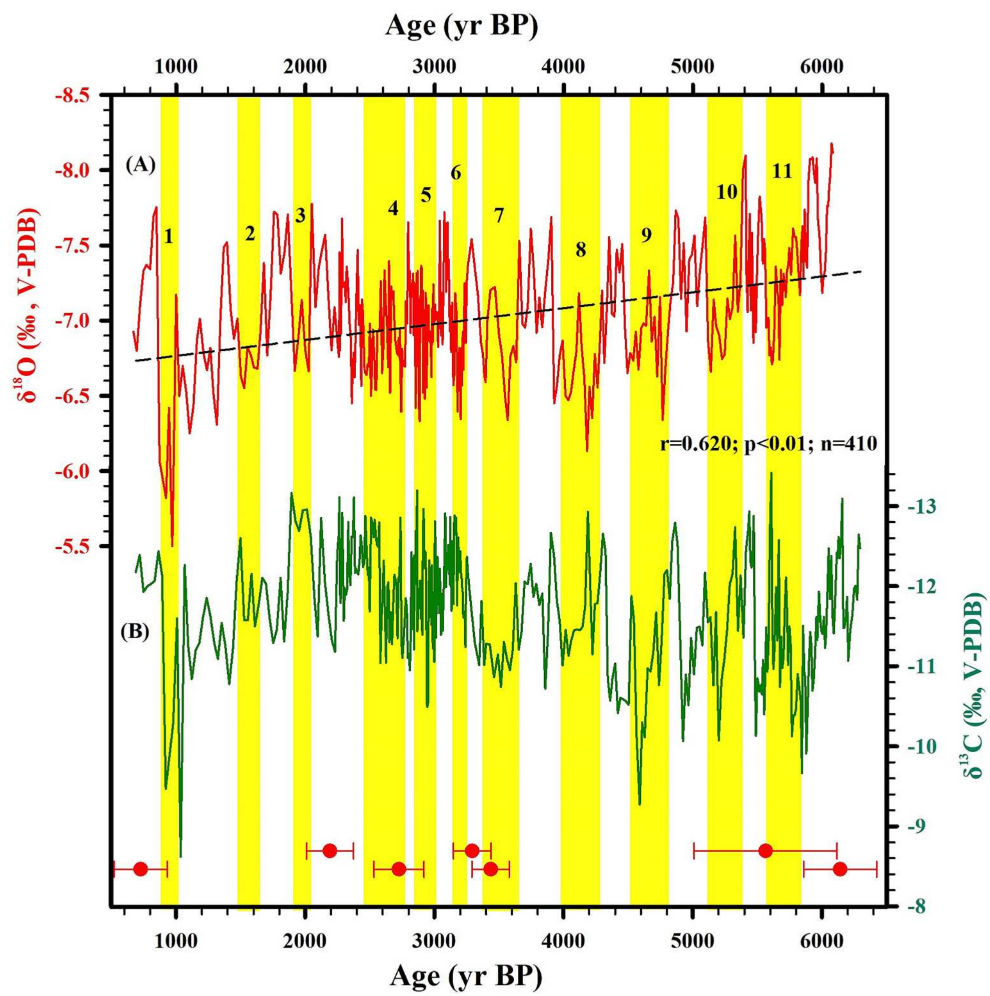

Fig. 4. $\delta^{18}O$ and $\delta^{13}C$ records of stalagmite FL2. (A) $\delta^{18}O$ record; the black dashed line is the trend line. (B) $\delta^{13}C$ record. The red dots at the bottom show the dating points with age errors. Yellow bands 1–11 represent eleven weak ASM events recorded by the $\delta^{18}O$ data. (For interpretation of the references to colour in this figure legend, the reader is referred to the web version of this article.)

5.2. Variation in the ASM during the middle and late Holocene

5.2.1. Regional comparison

Two main features can be identified based on the comparison between the $\delta^{18}O$ data of stalagmite FL2 and other stalagmite records in central and Southwest China. First, the intensity of the ASM exhibits a general decline during the middle to late Holocene (Wang et al., 2005; Zhao et al., 2017; Chen et al., 2021a; Li et al., 2021a,b) (Figs. 4 and 5). The $\delta^{18}O$ values of stalagmite FL2/DG/YL/FR/SB range from −8.17‰ to −5.5‰, −8.7‰ to −6.6‰, −12.3‰ to −8.8‰, −8.41‰ to −6.2‰, and − 10.5‰ to −8.0‰, respectively, and the $\delta^{18}O$ values fluctuate by an amplitude of 2–4‰ (maximum minus minimum for each record). Second, the $\delta^{18}O$ records of stalagmites from southwestern and central China record a series of weak ASM events on a centennial timescale

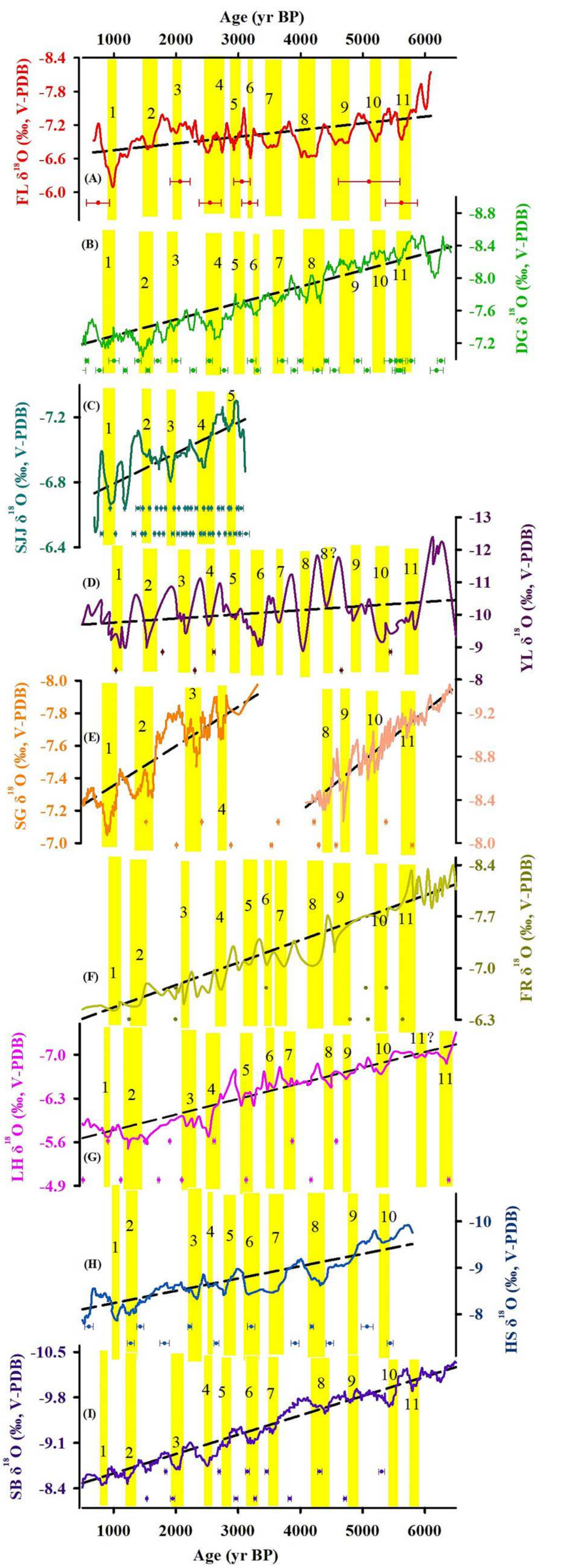

(caption on next column)

Fig. 5. Comparison of paleoclimate records from central and southwestern China during the middle and late Holocene. (A) FL2 (this study); (B) Dongge Cave (DG) (Wang et al., 2005); (C) Shijiangjun Cave (SJJ) (Chen et al., 2021a, 2021b); (D) Yelang Cave (YL) (Zhao et al., 2017); (E) Shigao Cave (SG) (Jiang et al., 2012); (F) Furong Cave (FR) (Li et al., 2021a); (G) Lianhua Cave (LH) (Zhang et al., 2013); (H) Heshang Cave (HS) (Hu et al., 2008); (I) Sanbao Cave (SB) (Dong et al., 2010). Yellow bands 1–11 represent eleven weak ASM events and the dashed black lines represent trend lines. (For interpretation of the references to colour in this figure legend, the reader is referred to the web version of this article.)

(Fig. 5). However, the age, duration, and magnitude of these weak summer monsoon events (WSME) differ among the different records (Fig. 5). For example, events 9–11 recorded by the $\delta^{18}O$ record of stalagmite FL2 have a longer duration and a larger variation than those recorded by stalagmite DA from Dongge cave (Fig. 5A and B), while other events recorded by the $\delta^{18}O$ values of stalagmite DA correspond well to the FL2 record. Although the high-precision stalagmite $\delta^{18}O$ record from the SJJ cave in western Guizhou covers only the last 3000 yr BP (Chen et al., 2021a), it also roughly records WSME 1–5 as stalagmite FL2 (Fig. 5A and C). The $\delta^{18}O$ records of the stalagmites from Furong cave in Southwest China and Lianhua cave, Heshang cave and Sanbao cave in central China also reveal a series of WSMEs similar to those recorded by FL2 (Fig. 5A, F, G, H and I). The differences in the dating errors, resolution of the stalagmite proxy records and their geographical setting may be the cause of the differences in the internal structure of these WSMEs (Duan et al., 2014). This does not change the two basic characteristics of summer monsoon variations recorded by stalagmites in central and Southwest China, namely, the overall weakening of the summer monsoon intensity and a series of WSMEs at the centennial scale (Fig. 5).

5.2.2. *Forcing of the weakened ASM*

The $\delta^{18}O$ records of stalagmite FL2 and other stalagmite records in the ASM region exhibit an overall positive trend during the MLH (Figs. 5 and 6), indicating that the ASM gradually weakened as the Northern Hemisphere temperature and summer insolation gradually decreased on a suborbital scale (Fig. 6A and G) (Wan et al., 2011; Cheng et al., 2016; Mohtadi et al., 2016).

The ITCZ is the main source of water vapor and heat in the Asian monsoon region and is caused by evaporation and convective activity in the tropical Indian and Pacific Oceans (Waliser and Gautier, 1993; Dong and Sutton, 2002; Bao, 2007; Griffiths et al., 2016). Ocean evaporation is directly influenced by the air temperature, sea-surface temperature and wind (Zhu et al., 1986; Zhang et al., 1996; Zhang et al., 2017). Since 6000 yr BP, the temperatures in the Northern Hemisphere have decreased by approximately 1.2 °C (Haug et al., 2001) (Fig. 6A). Changes in summer insolation in the Northern Hemisphere dominate the meridional temperature gradient between the Northern and Southern Hemispheres, resulting in shifts in the ITCZ, which impacts the strength of the ASM (Moy et al., 2002; Marcott et al., 2013; Wang et al., 2017; Tan et al., 2019). The change in the Ti content in Cariaco Basin sediments indicates that the ITCZ dramatically shifted southward during the middle to late Holocene (Fig. 6B) (Berkelhammer et al., 2014). The north–south shifts in the ITCZ position directly influence the amount of water vapor in the source region of the ASM. When the ITCZ moves southward, the convection of the ascending branch of the Hadley circulation in the Northern Hemisphere weakens (Schneider et al., 2014; Zhao et al., 2016), resulting in a weaker or more southerly ISM (Fig. 6D).

The activity and frequency of ENSO events have increased since 5000 yr BP (Fig. 6C) (Moy et al., 2002; Rein et al., 2005; Conroy et al., 2008; Toth et al., 2012; Zhang et al., 2014; Carré et al., 2014; Wu et al., 2019; Du et al., 2021). When an El Niño event occurs, the Walker Circulation weakens, and the ascending branch of the Walker Circulation in the Western Pacific Ocean moves eastward (Berkelhammer et al., 2014; Zhao et al., 2016). The warm surface waters of the western Pacific warm

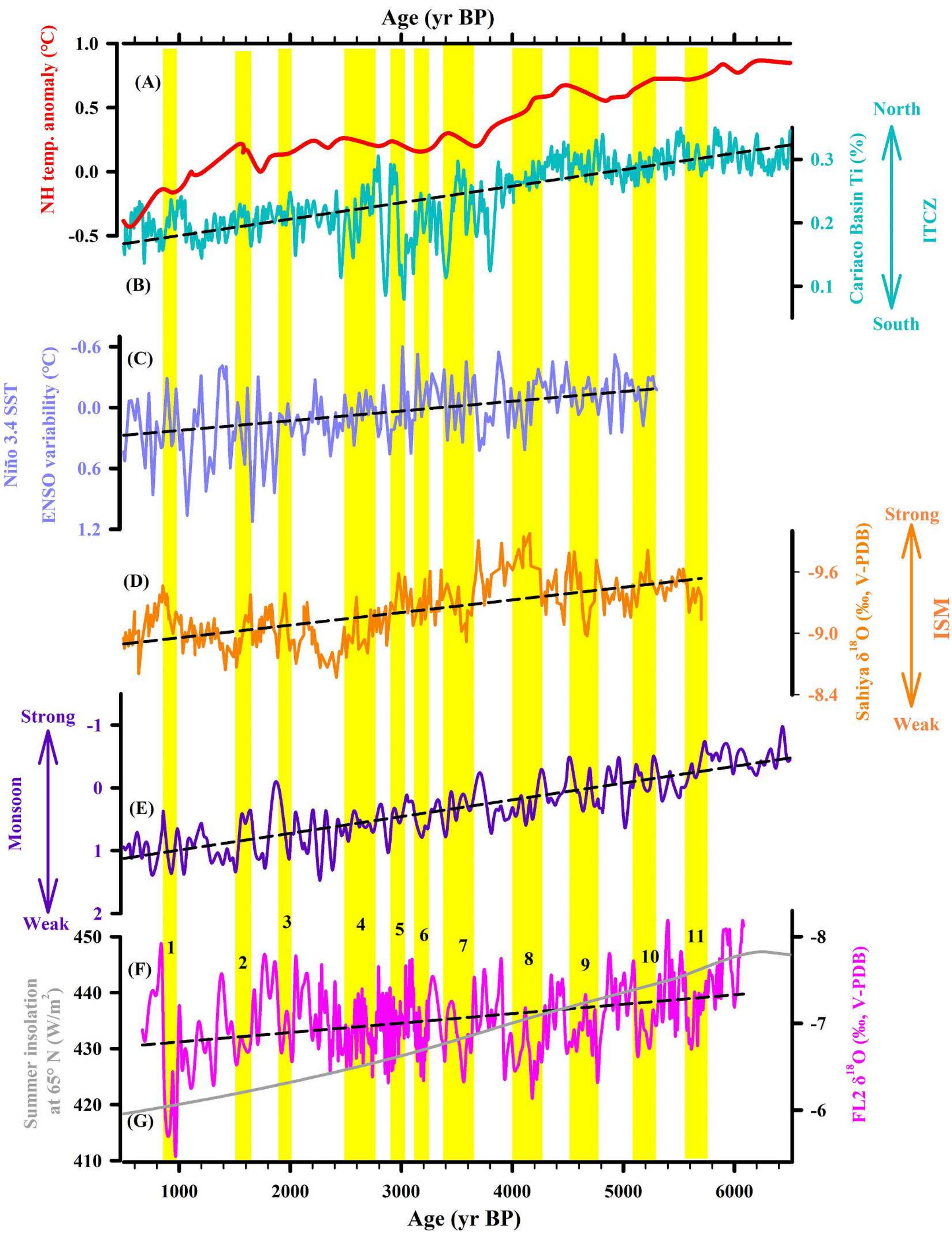

Fig. 6. Driving mechanism of the ASM during the middle and late Holocene. (A) The red curve is the index of temperature anomalies in the Northern Hemisphere (Marcott et al., 2013). (B) The blue–green curve is the Ti content in Cariaco Basin sediments (Haug et al., 2001), representing the north–south shift in the ITCZ. (C) The light purple curve is the simulated ENSO variability (Zhao et al., 2016). (D) The orange curve shows the $\delta^{18}O$ values of a stalagmite from Sahiya Cave, northern India, representing the intensity of the ISM (Kathayat et al., 2017). (E) The purple curve is the ASM intensity, PC1, of one transient simulation JJA precipitation (Jin et al., 2014). (F) The reddish-pink curve is the $\delta^{18}O$ values of stalagmite FL2. (G) The gray curve is the June–July August insolation at 65°N (Laskar et al., 2004). Yellow bands 1–11 mark weak ASM events recorded by the $\delta^{18}O$ values of stalagmite FL2. The dashed black lines represent trend lines for each record. (For interpretation of the references to colour in this figure legend, the reader is referred to the web version of this article.)

pool (WPWP) move eastward, and the extent of the warm pool decreases (Zhao et al., 2016; Chen and Li, 2018), which leads to a decrease in the surface temperature of the WPWP and a westward movement of the stronger western Pacific subtropical high (WPSH) (Wang et al., 2017; Chen and Li, 2018).Therefore, the intensity of the ASM is suppressed, the main water vapor source of precipitation in Southwest China is suppressed, and $\delta^{18}O$ values of precipitation increase (Mann and Jones, 2003; Schneider et al., 2014; Wang et al., 2017) (Fig. 6C, D, E and F).

5.3. Coupled variations in $\delta^{18}O$ and $\delta^{13}C$ and the evolution of the regional environment

There is a significant correlation between the $\delta^{18}O$ and $\delta^{13}C$ values of stalagmite FL2 ($r = 0.620$; $p < 0.01$; $n = 410$) (Fig. 4). This suggests that the $\delta^{13}C$ values of this stalagmite are closely related to the changes in the ASM on an interdecadal–centennial time scale. The $\delta^{13}C$ values of stalagmites are affected by biological and abiotic factors influenced by climate (Li et al., 2012a, 2018; Li and Li, 2018). Biological factors include the abundance of C3 and C4 plants (Cerling, 1984; Dorale et al., 1998; McDermott, 2004), changes in vegetation density and/or type of biomass (Li et al., 1997), soil microbial activity including the production of soil CO_2 (Baker et al., 1997; Li et al., 1997; Li et al., 2012a; Zhang, 2010; Liu et al., 2016), and changes in the atmospheric CO_2 concentration (Rudzka et al., 2011; Rampelbergh et al., 2014). Monitoring caves in Southwest China revealed that the $\delta^{13}C$ values of drip cave water are controlled by the amount of precipitation and its impact on soil biological processes, resulting in higher $\delta^{13}C_{DIC}$ values with decreasing precipitation and vice versa (Li and Li, 2018). Abiotic factors include the connectivity of bedrock fissures, ventilation in caves, and isotopic fractionation during carbonate deposition (Li et al., 2018). Higher/lower precipitation results in a weak/strong ventilation effect in the epikarst zone (Dreybrodt and Scholz, 2011), a shorten/extend the time of water–rock interaction (Baker et al., 1997; Oster et al., 2012), weak/strong prior calcite precipitation (PCP) (Hendy, 1971; Mickler et al., 2004; Liu et al., 2016), high/low CO_2 partial pressure in the cave air (Moros et al., 2004), weak/strong isotopic fractionation during the deposition of speleothems (Hall et al., 2004; Spötl et al., 2005; Li et al., 2012a), and lower/higher stalagmite $\delta^{13}C$ values (Li and Li, 2018). Both the $\delta^{18}O$ and $\delta^{13}C$ values are particularly high during the four major climatic events in the middle and late Holocene (~5500, 4200, and 2800 yr BP events and the MWP) (Fig. 4 and Fig. 7A). This suggests that the $\delta^{13}C$ values of the stalagmite are closely related to changes in the ASM on the interdecadal–centennial scale (Jones and Mann, 2004; Zhang et al., 2004; Kuo et al., 2011). The weakened ASM resulted in less precipitation, depressing the vegetation coverage/density, and finally leading to the deterioration of the karst ecological environment (Chen et al., 2021b).

The degradation of the karst environment indicated by the coupled change in stalagmite $\delta^{18}O$ and $\delta^{13}C$ values since the middle and late Holocene has also been observed in stalagmite records from other caves in Guizhou (Figs. 1 and 7). Based on this, we can assess the regional environmental evolution during the middle and late Holocene. For example, the $\delta^{13}C$ values of stalagmite DA in Dongge Cave are significantly biased in the 1–2‰ range during the events at ~5500 yr BP, 4200 yr BP, 2800 yr BP, and the MWP (Fig. 7H) (Duan et al., 2014). During the MWP, the $\delta^{13}C$ values of stalagmites were significantly higher in Zhijin Cave (Fig. 7E) (Kuo et al., 2011), Yelang Cave (Fig. 7F) (M. Zhao et al., 2017), Dongge Cave (Fig. 7G) (Duan et al., 2014), Wulu Cave (Fig. 7H) (Mohtadi et al., 2016), Longquan Cave (Fig. 7I) (Zhang et al., 2004), and Shigao Cave (Fig. 7J) (Yang et al., 2014).

With the onset of the Iron Age at ~3000 yr BP and the development of agriculture, the population in the Yangtze River Basin grew steadily, increasing from 16 million to 52 million during the period from 3000 to 750 yr BP, as revealed from the History Database of the Global Environment (HYDE 3.1) (Goldewijk et al., 2010; Pei et al., 2020) (Fig. 7D). This population growth profoundly affected the environment and its ecology. The $\delta^{13}C$ values of stalagmite FL2 positively changed by 4‰ in this period (Fig. 7A). Based on a reconstruction derived from the abundance of black carbon in sediment core ECMZ from the continental shelf of the East China Sea, the millennial scale reduction in regional fire activity since ~3000 yr BP was caused by a general decrease in forest coverage due to increasing human activity (Fig. 7B) (Pei et al., 2020). In contrast, the centennial scale increase in biomass burning usually coincided with periods characterized by increasing human activity associated with population migration or technological advances (Huang et al., 2014; Zhang et al., 2015a,b; Yuan et al., 2022). In addition, the abundance of microcharcoal in core GT-2 from a peat bog in southern China increased from 630 to 10,400 (grains/cm^2 yr) (Fig. 1, Fig. 7C), indicating increased fire activity in southern China since 1800 yr BP (Ma et al., 2018). All these lines of evidence point to a general decrease in forest coverage, a degradation of the regional environment and increasing human activities in the Yangtze River Basin and Southwest China in the late Holocene.

The MWP was an era of profound socioeconomic turbulence in China, and event 1 coincides with this period (Figs. 4 and 7). At the end of the Northern Song Dynasty (1127 CE), the army of the Jin Dynasty conquered Kaifeng City, the capital of the Northern Song Dynasty, and captured the Huizong and Qinzong emperors, resulting in the fall of the Northern Song Dynasty, which is known as the Jing-Kang event (JK event) in history (Dai and Bie, 2015). The JK event fundamentally changed the spatial pattern of Chinese society and the economy. After the JK event, the political and economic center shifted from the Yellow River Basin in northern China to the Yangtze River Basin in southern China (Dai and Bie, 2015) (Fig. 8), associated with a massive migration of people from northern to southern China (including Guizhou Province) (Zhang et al., 2004; Liu et al., 2011; Zhang et al., 2015a,b). From 1000 to 1150 CE D, the total population in the Yangtze River Basin increased from ~23 to ~52 million (Fig. 7D) (Goldewijk et al., 2010; Pei et al., 2020).

During the Northern Song Dynasty, the government set up Zunyi County in Yang's jurisdiction of Bozhou (1108 CE) (now Zunyi City, Guizhou province). Historical documents show that at the end of the Northern Song Dynasty the jurisdiction extent of Bozhou was mainly in northern Guizhou Province, and the population was less than ten thousand households (Zhang, 1980; Ma and Chen, 2015; Li, 2018a). In contrast, during the Southern Song Dynasty, the jurisdiction of Bozhou expanded to the south of the Wujiang River and into central and southern Guizhou Province (Fig. 8) (Zhang, 1980; Hou, 1996; Zhang, 2003). Subsequently, the Mongolian army invaded toward south China from Litang, Sichuan, conquered Dali country, stationed in Kunming, Xingyi and its surroundings, and finally invaded the middle and lower reaches of the Yangtze River from Guizhou to occupy the Southern Song Dynasty (1235 CE) (Fig. 8) (Wang and Li, 2021). A series of later wars resulted in large-scale migrations of people from northern to southern China, and increased human activities such as deforestation and land reclamation. This strong anthropogenic impact (Figs. 7 and 8) combined with the weak summer monsoon (Fig. 5A) led to an ecological deterioration in southwest Guizhou (Fig. 7).

Because of the differences in resolution, dating accuracy and the duration of available records (Figs. 4 and 5), detailed comparisons of changes in the karst environment in Southwest China are challenging. However, based on the analysis of available data, it can be confirmed that the weakening of the summer monsoon and the enhancement of human activity since the middle Holocene are recorded by the positive covariation of stalagmite $\delta^{18}O$ and $\delta^{13}C$ values (Li and Li, 2018; Chen et al., 2021b). It has been further confirmed that climate and human activities have controlled the evolution of the karst ecological environment (Chen et al., 2021b). Our study also confirms the hypothesis that the degradation of the regional karst environment was caused by climate change, social change and associated population increase (Chen et al., 2021b).

6. Conclusions

In this study, the evolution of the ASM and the regional karst environment during the middle to late Holocene (6270–670 yr BP) was reconstructed based on ^{230}Th dating and the $\delta^{18}O$ and $\delta^{13}C$ data of a stalagmite from Southwest China. During this period, the ASM experienced a weakening trend in response to decreased insolation, a southward migration of the ITCZ, and frequent El Niño events, as well as a superimposed series of interdecadal–centennial scale weak summer monsoon events.

The significant positive correlation between the $\delta^{18}O$ and $\delta^{13}C$ values of the stalagmite suggests that the karst ecological environment is sensitive to ASM changes. A comparative analysis of several stalagmite records from this region reveals that climatic events at ~5500 yr BP, 4200 yr BP, 2800 yr BP and during the MWP are consistently recorded, characterized by synchronous increases in the $\delta^{18}O$ and $\delta^{13}C$ values. These results indicate the changes in the karst hydrological conditions

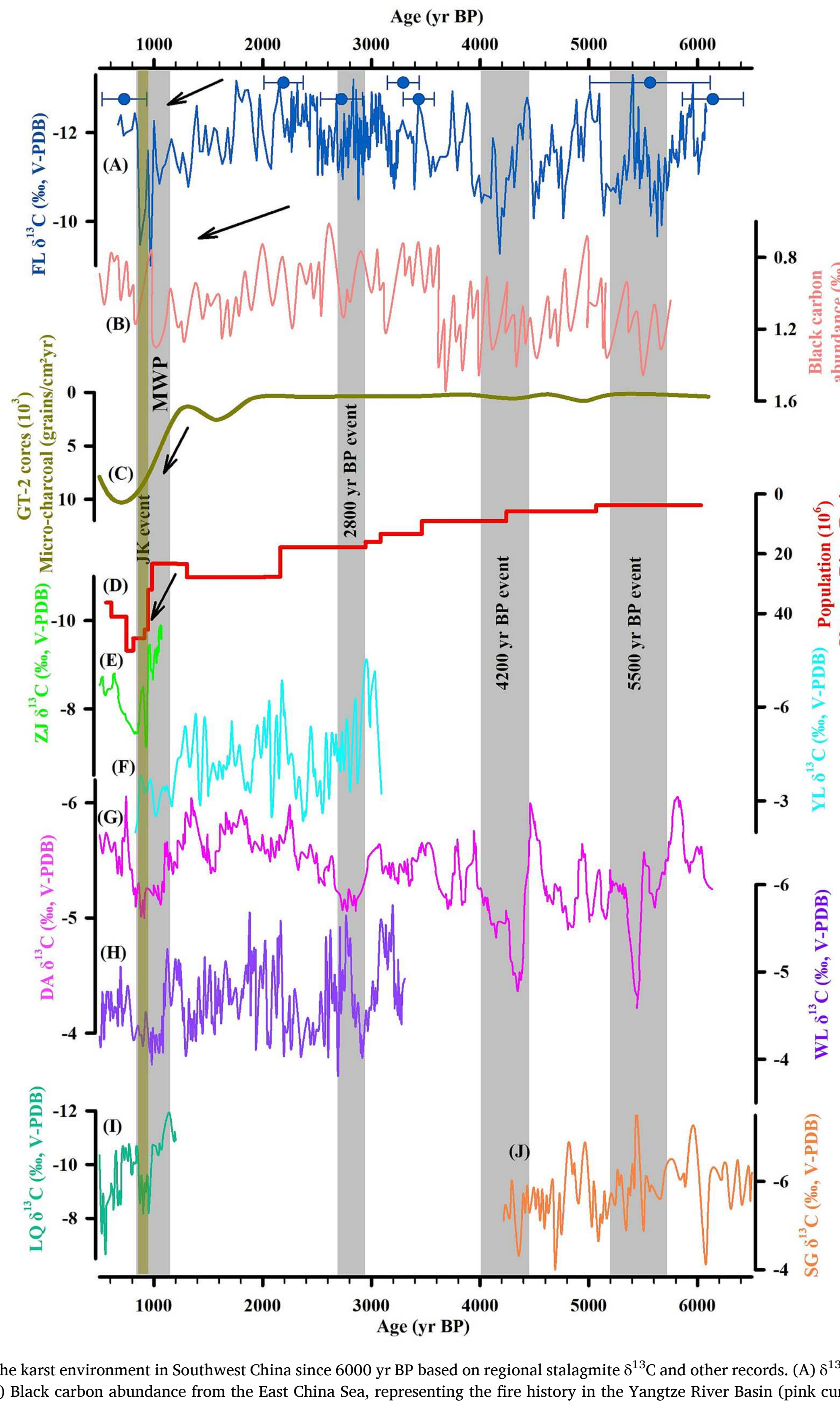

Fig. 7. Evolution of the karst environment in Southwest China since 6000 yr BP based on regional stalagmite $\delta^{13}C$ and other records. (A) $\delta^{13}C$ of stalagmite FL2 (blue curve, this study). (B) Black carbon abundance from the East China Sea, representing the fire history in the Yangtze River Basin (pink curve, Pei et al., 2020). (C) Microscopic charcoal influx recorded in the GT-2 core, representing the fire history in southern China (grass-green curve, Ma and Chen, 2015). (D) Population amount in the Yangtze River Basin (source: HYDE 3.1; red curve, Goldewijk et al., 2010; Pei et al., 2020); (E) Zhijin Cave (green curve, Kuo et al., 2011); (F) Yelang Cave (light blue curve, Zhao et al., 2017); (G) Dongge Cave (reddish-pink curve, Wang et al., 2005); (H) Wulu Cave (purple curve, Mohtadi et al., 2016); (I) Longquan Cave (blue green curve, Zhang et al., 2004); (J) Shigao Cave (orange curve, Yang et al., 2014). The gray bands represent the MWP, 2.8 ka event, 4.2 ka event, and 5.5 ka event. The grass-green band represents the Jing-Kang event (JK event). (For interpretation of the references to colour in this figure legend, the reader is referred to the web version of this article.)

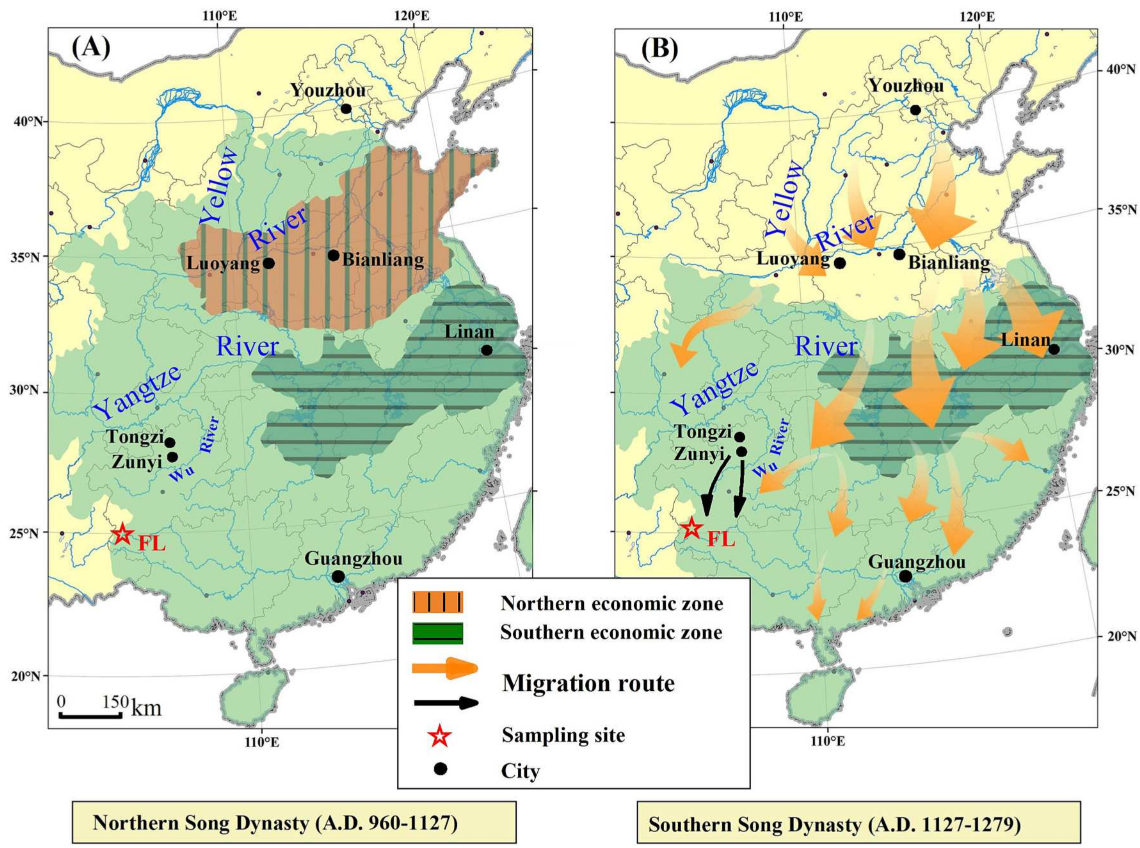

Fig. 8. Changes in the extent of the Northern Song Dynasty and Southern Song Dynasty (modified after Dai and Bie, 2015). (A) Territory of the Northern Song Dynasty (light green area). The middle and lower reaches of the Yellow River Basin and the Yangtze River Basin were controlled by the Northern Song Dynasty, and the political and economic center of ancient Chinese civilization was located in the Yellow River Basin (orange area) and the Yangtze River Basin (dark green area). The black dots represent important cities during the Song Dynasty. Bianliang was the capital of the Northern Song Dynasty (now Kaifeng City). Linan was the capital of the Southern Song Dynasty (now Hangzhou City). The red star indicates the location of FL Cave (this study). (B) Territory of the Southern Song Dynasty (light green area). The northern Yellow River Basin economic zone was separated from the Southern Song Dynasty. The black arrows represent the expansion route of Yang's rule from Bozhou to southwestern Guizhou (Zhang, 2003). The orange arrows represent the migration routes into southern China after the Jing-Kang event (Dai and Bie, 2015). (For interpretation of the references to colour in this figure legend, the reader is referred to the web version of this article.)

and the degradation of vegetation and soil biological processes in Southwest China induced by ASM weakening. Therefore, the weakening of the summer monsoon and the sustained growth and southward migration of the Chinese population may have eventually caused the deterioration of the ecological environment in the karst regions of Southwest China since the middle Holocene.

Supplementary data to this article can be found online at https://doi.org/10.1016/j.palaeo.2023.111437.

Authorship contribution statement

T.-Y Li and J.-Y Li obtained funding, conducted fieldwork, conceptualized this study and revised the manuscript. R.D. wrote the original draft. C.S., H.-C. L., H.-B.W., H.C., Y.F.N., C.-C.S., J.-L. Z., C.-J.C., R.L.E., and Z.-Q.L. carried out sampling, ^{230}Th dating and data analysis, and contributed to the final manuscript.

Declaration of Competing Interest

The authors declare no conflict of interest.

Data availability

The data will be reserved in a public data base and completely share to public freely.

Acknowledgments

This research was supported by the National Natural Science Foundation of China (NSFC, No. 42172204; 42011530078; 41888101; 42272214) to J.-Y Li, T.-Y Li, and H. Cheng, and Yunnan Fundamental Research Projects (grant no. 202201AS070022) and the Reserve talent of the Young and Middle-age Academic and Technical Leader in Yunnan Province (No. 202205AC160025) to T.-Y Li. This study was also supported by grants from the Science Vanguard Research Program of the Ministry of Science and Technology (MOST), Taiwan, ROC (110-2123-M-002-009 to C.-C.S.), the Higher Education Sprout Project of the Ministry of Education, Taiwan, ROC (110L901001 to C.-C.S.), and National Taiwan University (110L8907 to C.-C.S.), and U.S. NSF 2202913 to RLE.

References

Baker, A., Ito, E., Smart, P.L., Mcewan, R.F., 1997. Elevated and variable values of ^{13}C in speleothems in a british cave system. Chem. Geol. 136, 263–270.
Bao, M., 2007. The statistical analysis of the persistent heavy rain in the last 50 years over China and their backgrounds on the large-scale circulation. Chin. J. Atmos. Sci. 31, 779–792.
Berkelhammer, M., Sinha, A., Mudelsee, M., Cheng, H., Yoshimura, K., Biswas, J., 2014. On the low-frequency component of the ENSO-Indian monsoon relationship; a paired proxy perspective. Clim. Past 10, 733–744.
Carré, M., Sachs, J.P., Purca, S., Schauer, A.J., Braconnot, P., Angeles Falcon, R., et al., 2014. Holocene history of ENSO variance and asymmetry in the eastern tropical Pacific. Science 345 (6200), 1045–1048.

Cerling, T.E., 1984. The stable isotopic composition of soil carbonate and its relationship to climate. Earth Planet. Sci. Lett. 71, 229–240.
Chen, C.-J., Li, T.-Y., 2018. Geochemical characteristics of cave drip water respond to ENSO based on a 6-year monitoring work in Yangkou Cave, Southwest China. J. Hydrol. 561, 896–907.
Chen, C.-J., Huang, R., Yuan, D.-X., Zhang, J., Cheng, H., Ning, Y.-F., Yu, T.-L., Shen, C.-C., Edwards, R.L., Long, X.-Y., Wang, T., Xiao, S.-Y., Wu, Y., Liu, Z.-Q., Li, T.-Y., Li, J.-Y., 2021a. Karst hydrological changes during the Late-Holocene in Southwest China. Quat. Sci. Rev. 258, 106865.
Chen, C.-J., Yuan, D.-X., Cheng, H., Yu, T.L., Shen, C.-C., Edwards, R.L., Wu, Y., Xiao, S.-Y., Zhang, J., Wang, T., Huang, R., Liu, Z., Li, T.-Y., Li, J.-Y., 2021b. Human activity and climate change triggered the expansion of rocky desertification in the karst areas of Southwest China. Sci. China Earth Sci. 64, 1761–1773.
Cheng, H., Edwards, R.L., Shen, C.-C., Polyak, V.J., Asmerom, Y., Woodhead, J., Hellstrom, J., Wang, Y.-J., Kong, X.-G., Spötl, C., Wang, X.F., 2013. Improvements in ^{230}Th dating, ^{230}Th and ^{234}U half-life values, and U-Th isotopic measurements by multicollector inductively coupled plasma mass spectroscopy. Earth Planet. Sci. Lett. 371–372, 82–91.
Cheng, H., Edwards, R.L., Sinha, A., Spötl, C., Yi, L., Chen, S.T., Kelly, M., Kathayat, G., Wang, X.F., Li, X.L., Kong, X.G., Wang, Y.J., Ning, Y.F., Zhang, H.W., 2016. The asian monsoon over the past 640,000 years and ice age terminations. Nature 534, 640–646.
Cheng, H., Sinha, A., Wang, X.F., Cruz, F.W., Edwards, R.L., 2012. The Global Paleomonsoon as seen through speleothem records from Asia and the Americas. Clim. Dyn. 39, 1045–1062.
Cheng, H., Zhang, H.W., Zhao, J.Y., Li, H.Y., Ning, Y.F., Kathayat, G., 2019. Chinese stalagmite paleoclimate researches, a review and perspective. Sci. China Earth Sci. 62, 1489–1513.
Cheng, Q.P., Gao, L., Zhong, F.L., Zuo, X.A., Ma, M.M., 2020. Spatiotemporal variations of drought in the Yunnan-Guizhou Plateau, Southwest China, during 1960–2013 and their association with large-scale circulations and historical records. Ecol. Indic. 112, 106041.
Conroy, J.L., Overpeck, J.T., Cole, J.E., Shanahan, T.M., Steinitz-Kannan, M., 2008. Holocene changes in eastern tropical Pacific climate inferred from a Galápagos lake sediment record. Quat. Sci. Rev. 27 (11–12), 1166–1180.
Cosford, J., Qing, H.-R., Eglington, B., Mattey, D., Yuan, D.-X., Zhang, M.-L., Cheng, H., 2008. East asian monsoon variability since the Mid-Holocene recorded in a high resolution, absolute-dated aragonite speleothem from eastern China. Earth Planet. Sci. Lett. 275, 296–307.
Dai, Q., Bie, C.X., 2015. The economic consequence of financial pressure, take the change of "Jing-Kang event" in Song Dynasty as an example (in Chinese). J. World Econ. 38, 173–192.
Dayem, K.E., Molnar, P., Battisti, D.S., Roe, G.H., 2010. Lessons learned from oxygen isotopes in modern precipitation applied to the interpretation of speleothem records of paleoclimate from eastern Asia. Earth Planet. Sci. Lett. 295, 219–230.
Dong, B.W., Sutton, R.T., 2002. Adjustment of the coupled ocean-atmosphere system to a sudden change in the thermohaline circulation. Geophys. Res. Lett. 29, 18-1-18-4.
Dong, J.G., Wang, Y.J., Cheng, H., Hardt, B., Edwards, R.L., Kong, X.G., Wu, J.Y., Chen, S.T., Liu, D.B., Jiang, X.Y., Zhao, K., 2010. A high-resolution stalagmite record of the Holocene East asian monsoon from Mt Shennongjia, Central China. The Holocene 20, 257–264.
Dorale, J.A., Edwards, R.L., Ito, E., González, L.A., 1998. Climate and vegetation history of the midcontinent from 75 to 25 ka, a speleothem record from crevice cave, Missouri, USA. Science 282, 1871–1874.
Dorale, J.A., Liu, Z.H., 2009. Limitations of Hendy Test criteria in judging the paleoclimatic suitability of speleothems and the need for replication. J. Cave Karst Stud. 71, 73–80.
Dreybrodt, W., Scholz, D., 2011. Climatic dependence of stable carbon and oxygen isotope signals recorded in speleothems, from soil water to speleothem calcite. Geochim. Cosmochim. Acta 75, 734–752.
Du, X.J., Hendy, I., Hinnov, L., Brown, E., Zhu, J., Poulsen, C.J., 2021. High-resolution interannual precipitation reconstruction of Southern California: Implications for Holocene ENSO evolution. Earth Planet Sci. Lett. 554, 116670.
Duan, F.C., Wang, Y.J., Shen, C.C., Wang, Y., Cheng, H., Wu, C.C., Hu, H.M., Kong, X.G., Liu, D.B., Zhao, K., 2014. Evidence for solar cycles in a late Holocene speleothem record from Dongge Cave China. Sci. Rep. 4, 5159.
Edwards, R.L., Chen, J.H., Wasserburg, G.J., 1987. ^{238}U–^{234}U-^{230}Th-^{232}Th systematics and the precise measurement of time over the past 500,000 years. Earth Planet. Sci. Lett. 81, 175–192.
Fairchild, I.J., Smith, C.L., Baker, A., Fuller, L., Spötl, C., Mattey, D., McDermott, F., E.I. M.F., 2006. Modification and preservation of environmental signals in speleothems. Earth-Sci. Rev. 75, 105–153.
Fang, X.Q., Su, Y., Yin, J., Teng, J.C., 2015. Transmission of climate change impacts from temperature change to grain harvests, famines and peasant uprisings in the historical China. Sci. China Earth Sci. 58, 1427–1439.
Goldewijk, K.K., Beusen, A., Janssen, P., 2010. Long-term dynamic modeling of global population and built-up area in a spatially explicit way, HYDE 3.1. The Holocene 20, 565–573.
Griffiths, M.L., Kimbrough, A.K., Gagan, M.K., Drysdale, R.N., Cole, J.E., Johnson, K.R., Zhao, J.X., Cook, B.I., Hellstrom, J.C., Hantoro, W.S., 2016. Western Pacific hydroclimate linked to global climate variability over the past two millennia. Nat. Commun. 7, 11719.
Guo, C.Q., Zhou, R., Pan, L.Y., 2015. Analysis of drought and flood disasters in karst area of Southwest China from 1900 to 2012. J. Water Resour. Water 26, 12–15.
Guo, W., Li, D.H., Yang, W.C., 2006. Comparative research on Mollusca, arthropoda and chordata communities in Xia cave, Feilong cave and Bailong cave in Xingyi (in Chinese). Guizhou Sci. 02, 48–55.
Hall, I.R., Bianchi, G.G., Evans, J.R., 2004. Centennial to millennial scale Holocene climate-deep water linkage in the North Atlantic. Quat. Sci. Rev. 23, 1529–1536.
Haug, G., Hughen, K., Sigman, D., Peterson, L., Röhl, U., 2001. Southward migration of the intertropical convergence zone through the Holocene. Science 293, 1304–1308.
Hendy, C.H., 1971. The calculation of the effects of different modes of formation on the isotopic composition of speleothems and their applicability as palaeoclimate indicators. Geochim. Cosmochim. Acta 35, 801–824.
Hercman, H., Pawlak, J., 2012. MOD-AGE, an age-depth model construction algorithm. Geochronology 12, 1–10.
Hou, S.Z., 1996. The contribution of Bozhou army and civilians in fighting against Jin Meng (Yuan) in song Dynasty (in Chinese). J. Guizhou Norm. Univ. (Soc. Sci.) 4, 30–33.
Hu, C.Y., Henderson, G.M., Huang, J.H., Xie, S.C., Sun, Y., Johnson, K.R., 2008. Quantification of Holocene asian monsoon rainfall from spatially separated cave records. Earth Planet. Sci. Lett. 266, 221–232.
Huang, K.Y., Zheng, Z., Liao, W.B., Cao, L.L., Zheng, Y.W., Zhang, H., Zhu, G.Q., Zhang, Z., Cheddadi, R., 2014. Reconstructing late Holocene vegetation and fire histories in monsoonal region of southeastern China. Palaeogeogr. Palaeoclimatol. Palaeoecol. 393, 102–110.
Jaffey, A.H., Flynn, K.F., Glendenin, L.E., Bentley, W.C., Essling, A.M., 1971. Precision measurement of half-lives and specific activities of ^{235}U and ^{238}U. Phys. Rev. C 4, 1889–1906.
Jiang, X.Y., He, Y.Q., Shen, C.C., Kong, X.G., Li, Z.Z., Chang, Y.W., 2012. Stalagmite-inferred Holocene precipitation in northern Guizhou Province, China, and asynchronous termination of the Climatic Optimum in the Asian monsoon territory. Chin. Sci. Bull. 57, 73–79.
Jiang, Z.C., Luo, W.Q., Tong, L.Q., Cheng, Y., Yang, Q.Y., Wu, Z.Y., Liang, J.H., 2016. Evolution features of rocky desertification and influence factors in karst areas of Southwest China in the 21st century. Carsol. Sin. 35, 461–468.
Jin, L.Y., Schneider, B., Park, W.S., Latif, M., Khon, V., Zhang, X.J., 2014. The spatial-temporal patterns of asian summer monsoon precipitation in response to Holocene insolation change, a model-data synthesis. Quat. Sci. Rev. 85, 47–62.
Jones, P.D., Mann, M.E., 2004. Climate over past millennium. Rev. Geophys. 42, 1–42.
Kathayat, G., Cheng, H., Sinha, A., Yi, L., Li, X.L., Zhang, H.W., Li, H.Y., Ning, Y.F., Edwards, R.L., 2017. The indian monsoon variability and civilization changes in the indian subcontinent. Sci. Adv. 3, 1701296.
Kuo, T.-S., Liu, Z.-Q., Li, H.-C., Wan, N.-J., Shen, C.-C., Ku, T.-L., 2011. Climate and environmental changes during the past millennium in central western Guizhou, China as recorded by Stalagmite ZJD-21. J. Asian Earth Sci. 40, 1111–1120.
Laskar, J., Robutel, P., Joutel, F., Gastineau, M., Correia, A.C.M., Levrard, B., 2004. A long-term numerical solution for the insolation quantities of the Earth. Astron. Astrophys. 42, 261–285.
Li, T.-Y., Li, H.-C., Xiang, X.-J., Guo, Z.-X., Li, J.-Y., Zhou, F.-L., Chen, H.-L., Peng, L.-L., 2012a. Transportation characteristics of δ^{13}C in the plants-soil-bedrock-cave system in Chongqing karst area. Sci. China Earth Sci. 55, 685–694.
Li, F., 2018a. A review about Yang family's discovery and research (in Chinese). Guizhou Cult. Hist. 02, 7–18.
Li, H.-C., Gu, D.-L., Stott, L.-D., Yuan, D.-X., Chen, W.-J., Li, T.-Y., 1997. Interannual-resolution δ^{13}C record of stalagmites as proxy for the changes in precipitation and atmospheric CO_2 in Shihua cave, Beijing. Carsol. Sin. 16, 285–295. (In Chinese with English abstract and figures).
Li, J.-Y., Li, T.-Y., 2018. Seasonal and annual changes in soil/cave air pCO_2 and the δ^{13}C DIC of cave drip water in response to changes in temperature and rainfall. Appl. Geochem. 93, 94–101.
Li, T.-Y., 2018b. False amount effect—A discussion on one issue of isotopic climatology. Quat. Sci. 38, 1545–1548.
Li, T.-Y., Wu, Y., Shen, C.-C., Li, J.-Y., Chiang, H.-W., Lin, K., Tan, L.-C., Jiang, X.-Y., Cheng, H., Edwards, R.L., 2021a. High precise dating on the variation of the asian summer monsoon since 37 ka BP. Sci. Rep. 11, 9375.
Li, Z.X., He, Y.Q., Wang, P.Y., Theakstone, W.H., An, W.L., Wang, X.F., Lu, A.G., Zhang, W., Cao, W.H., 2012b. Changes of daily climate extremes in Southwest China during 1961–2008. Glob. Planet. Chang. 80, 255–272.
Li, T.-Y., Huang, C.-X., Tian, L.J., Suarez, M., Gao, Y.L., 2018. Variation of δ^{13}C in plant-soil-cave systems in karst regions with different degrees of rocky desertification in Southwest China and implications for paleoenvironment reconstruction. J. Cave Karst Stud. 80 (4), 212–228.
Liu, D.B., Wang, Y.J., Cheng, H., Edwards, R.L., Kong, X.G., Li, T.-Y, 2016. Strong coupling of centennial-scale changes of asian monsoon and soil processes derived from stalagmite δ^{18}O and δ^{13}C records, southern China. Quat. Res. 85, 333–346.
Li, T.-Y., Xiao, S.-Y., Shen, C.-C., Zhang, J., Chen, C.-J., Cheng, H., Spötl, C., Huang, R., Wang, T., Li, J.-Y., Wu, Y., Liu, Z.Q., Edwards, R.L., Yu, T.-L., 2021b. Little Ice Age climate changes in Southwest China from a stalagmite δ^{18}O record. Palaeogeogr. Palaeoclimatol. Palaeoecol. 562, 110167.
Liu, Z.-H., Sun, H.-L., Li, H.-C., Wan, N.-J., 2011. δ^{13}C, δ^{18}O and deposition rate of tufa in Xiangshui River, SW China, Implications for land-cover change caused by climate and human impact during the late Holocene. Geol. Soc. Lond. Spec. Publ. 352, 85–96.
Liu, Z.-Q., Li, H.-C., Xiong, K.-N., Yuan, D.-X., Ying, B., Xu, X.-M., Li, J.-Y., 2008. Implication for sampling paleo-climate indicators by monitoring seasonal variations of δD and δ^{18}O in cave waters. Carsol. Sin. 2, 139–144. (In Chinese with English abstrct and figures).

Ma, G.J., Chen, D.M., 2015. On the governance to South-western parts in the Yuan, Ming and Qing dynasties from the change of the Yang Clan's jurisdiction (in Chinese). J. Zunyi Norm. Univ. 17 (02), 7–12.
Ma, T., Zheng, Z., Man, M., Dong, Y.X., Li, J., Huang, K.Y., 2018. Holocene fire and forest histories in relation to climate change and agriculture development in southeastern China. Quat. Int. 488, 30–40.
Mann, M.E., Jones, P.D., 2003. Jones Global surface temperatures over the past two millennia. Geophys. Res. Lett. 30, 1820.
Marcott, S.A., Shakun, J.D., Clark, P.U., Mix, A.C., 2013. A reconstruction of regional and global temperature for the past 11,300 years. Science 339, 1198–1201.
McDermott, F., 2004. Palaeo-climate reconstruction from stable isotope variations in speleothems, a review. Quat. Sci. Rev. 23, 901–918.
Mickler, P.J., Banner, J.L., Stern, L., Asmerom, Y., Edwards, R.L., Ito, E., 2004. Stable isotope variations in modern tropical speleothems, evaluating equilibrium vs. Kinetic isotope effects. Geochim. Cosmochim. Acta 68, 4381–4393.
Mohtadi, M., Prange, M.S., Steinke, S., 2016. Palaeoclimatic insights into forcing and response of monsoon rainfall. Nature 533, 191–199.
Moros, M., Emeis, K.C., Risebrobakken, B., Snowball, I., Kuijpers, A., Mcmanus, J., Jansen, E., 2004. Sea surface temperatures and ice rafting in the Holocene North Atlantic, climate influences on northern Europe and Greenland. Quat. Sci. Rev. 23, 2113–2126.
Moy, C.M., Seltzer, G.O., Rodbell, D.T., Anderson, D.M., 2002. Variability of El Niño/Southern oscillation activity at millennial timescales during the Holocene epoch. Nature 420, 162–165.
Oster, J.L., Montañez, I.P., Kelley, N.P., 2012. Response of a modern cave system to large seasonal precipitation variability. Geochim. Cosmochim. Acta 91, 92–108.
Pausata, F.S.R., Battisti, D.S., Nisancioglu, K.H., Bitz, C.M., 2011. Chinese stalagmite $\delta^{18}O$ controlled by changes in the indian monsoon during a simulated Heinrich event. Nat. Geosci. 4, 474–480.
Pei, W.Q., Wan, S.M., Clift, P.D., Dong, J., Liu, X.T., Lu, J., Tan, Y., Shi, X.F., Li, A.C., 2020. Human impact overwhelms long-term climate control of fire in the Yangtze River Basin since 3.0 ka BP. Quat. Sci. Rev. 230, 106165.
Rampelbergh, M.V., Verheyden, S., Allan, M., Quinif, Y., 2014. Monitoring of a fast-growing speleothem site from the Han-sur-Lesse cave, Belgium, indicates equilibrium deposition of the seasonal $\delta^{18}O$ and $\delta^{13}C$ signals in the calcite. Clim. Past 10, 1871–1885.
Rehfeld, K., Marwan, N., Breitenbach, S.F.M., Kurths, J., 2013. Late Holocene asian summer monsoon dynamics from small but complex networks of paleoclimate data. Clim. Dyn. 41, 3–19.
Rein, B., Lückge, A., Reinhardt, L., Sirocko, F., Wolf, A., Dullo, W.C., 2005. El Niño variability off Peru during the last 20,000 years. Paleoceanography 20 (4).
Ruan, J.Y., Zhang, H.Y., Cai, Z.Y., Yang, X.Q., Yin, J., 2019. Regional controls on daily to interannual variations of precipitation isotope ratios in Southeast China: implications for paleomonsoon reconstruction. Earth Planet. Sci. Lett. 527, 115794.
Rudzka, D., McDermott, F., Baldini, L.M., Fleitmann, D., Moreno, A., Stoll, H., 2011. The coupled $\delta^{13}C$ radiocarbon systematics of three late Glacial/early Holocene speleothems, Insights into soil and cave processes at climatic transitions. Geochim. Cosmochim. Acta 75, 4321–4339.
Schneider, T., Bischoff, T., Haug, G.H., 2014. Migrations and dynamics of the intertropical convergence zone. Nature 513, 45–53.
Scholz, D., Hoffmann, D., 2011. StalAge: an algorithm designed for construction of speleothem age models. Quat. Geochronol. 6 (3–4), 369–382.
Shen, C.-C., Wu, C.-C., Cheng, H., Edwards, R.L., Hsieh, Y.-T., Gallet, S., Chang, C.-C., Li, T.-Y., Lam, D.-D., Kano, A., Hori, M., Spötl, C., 2012. High-precision and high-resolution carbonate ^{230}Th dating by MC-ICP-MS with SEM protocols. Geochim. Cosmochim. Acta 99, 71–86.
Spötl, C., Fairchild, I., Tooth, A.F., 2005. Cave air control on dripwater geochemistry, Obir Caves Austria, implications for speleothem deposition in dynamically ventilated caves. Geochim. Cosmochim. Acta 69, 2451–2468.
Spötl, C., Vennemann, T., 2003. Continuous-flow isotope ratio mass spectrometric analysis of carbonate minerals. Rapid Communication in Mass Spectrometry 17, 1004–1006.
Tan, L.C., Cai, Y.J., Cheng, H., Edwards, R.L., Lan, J.G., Zhang, H.W., Li, D., Ma, L., Zhao, P.P., Guo, Y.L., 2018. High resolution monsoon precipitation changes on southeastern Tibetan Plateau over the past 2300 years. Quat. Sci. Rev. 195, 122–132.
Tan, L.C., Shen, C.C., Löwemark, L., Wohlfarth, B., 2019. Rainfall variations in central Indo-Pacific over the past 2,700 y. Proc. Natl. Acad. Sci. USA 116, 17201–17206.
Tan, M., 2009. Circulation effect, climatic significance of the short-term variability of the oxygen isotopes in stalagmites from monsoonal China. Quat. Sci. 29, 851–862.
Tan, M., 2014. Circulation effect, response of precipitation $\delta^{18}O$ to the ENSO cycle in monsoon regions of China. Clim. Dyn. 42, 1067–1077.
Tan, M., 2016. Circulation background of climate patterns in the past millennium, uncertainty analysis and re-reconstruction of ENSO-like state. Sci. China Earth Sci. 59, 1225–1241.
Toth, L.T., Aronson, R.B., Vollmer, S.V., Hobbs, J.W., Urrego, D.H., Cheng, H., et al., 2012. ENSO drove 2500-year collapse of eastern Pacific coral reefs. Science 337 (6090), 81–84.
Waliser, D.E., Gautier, C., 1993. A satellite-derived climatology of the ITCZ. J. Clim. 6, 2162–2174.
Wan, N.-J., Li, H.-C., Liu, Z.-Q., Yang, H.-Y., Yuan, D.-X., Chen, Y.-H., 2011. Spatial variations of monsoonal rain in eastern China, instrumental, historic and speleothem records. J. Asian Earth Sci. 40, 1139–1150.
Wang, P.X., Wang, B., Cheng, H., Fasullo, J., Guo, Z.T., Kiefer, T., Liu, Z.Y., 2017. The global monsoon across time scales, Mechanisms and outstanding issues. Earth Sci. Rev. 174, 84–121.
Wang, X.P., Li, Z.H., 2021. Kublai khan and the battles of Xiangfang in the Song Dynasty and the Yuan Dynasty (in Chinese). J. Hubei Univ. Arts Sci. 42, 17–20.
Wang, Y.J., Cheng, H., Edwards, R.L., He, Y.Q., Kong, X.G., An, Z.S., Wu, J.Y., Kelly, M. J., Dykoski, C.D., Li, X.D., 2005. The Holocene asian monsoon, Links to solar changes and North Atlantic climate. Science 308, 854–857.
Wang, Y.J., Cheng, H., Edwards, R.L., An, Z.S., Wu, J.Y., Shen, C.C., Dorale, J.A., 2001. A high-resolution absolute-dated late Pleistocene monsoon record from Hulu Cave, China. Science 294, 2345–2348.
Wu, J., Liu, Q., Cui, Q.Y., Xu, D.K., Wang, L., Shen, C.M., Chu, G.Q., Liu, J.Q., 2019. Shrinkage of East Asia Winter Monsoon Associated with increased ENSO events since the Mid-Holocene. J. Geophys. Res. Atmos. 124, 3839–3848.
Wu, S.D., 2000. The History of Population of China: Liao, Song, Jin and Yuan Dynasties (in Chinese). In: Fudan University Press, Shanghai, pp. 314–500.
Wu, Y., Li, T.-Y., Yu, T.-L., Shen, C.-C., Chen, C.-J., Zhang, J., Li, J.-Y., Wang, T., Huang, R., Xiao, S.-Y., 2020. Variation of the Asian summer monsoon since the last glacial-interglacial recorded in a stalagmite from Southwest China. Quat. Sci. Rev. 234, 106261.
Wu, Y., Li, T.-Y., Li, J.-Y., Cheng, H., Ning, H.F., Shen, C.-C., Yang, Y., Zhao, J.Y., Chen, C.J., Liang, M.Q., Xiao, S.Y., Qiu, H.Y., Xu, Y.Z., Huang, Y.Y., Yu, T.L., Edwards, R.L., 2023. Variations in Asian summer monsoon and hydroclimate during Heinrich stadials 4 revealed by stalagmite stable isotopes and trace elements. Quat. Sci. Rev. 299, 107869.
Xiao, X.Y., Haberle, S.G., Shen, J., Yang, X.D., Han, Y., Zhang, E.L., Wang, S.M., 2014. Latest Pleistocene and Holocene vegetation and climate history inferred from an alpine lacustrine record, northwestern Yunnan Province, Southwest China. Quat. Sci. Rev. 86, 35–48.
Yassoglou, N.J., 2000. History of desertification in the European Mediterranean. In: Enne, G., D'Angelo, M., Zanolla, C. (Eds.), Indicators for Assessing Desertification in the Mediterranean. Proceedings of the International Seminar. University of Sassari Nucleo Ricerca Desertificazion, Sassari, pp. 9–15.
Yang, B., Lei, G.L., Jiang, X.Y., 2014. 9.9~4.2 ka BP stalagmite trace elements records from Shigao cave, northern Guizhou province and its environmental significance. Marine Geol. Quat. Geol. 34, 143–148.
Yuan, Z.J., Wu, D., Wang, T., Ma, X.Y., Li, Y.M., Shao, S., Zhang, Y., Zhou, A.F., 2022. Holocene fire history in southwestern China linked to climate change and human activities. Quat. Sci. Rev. 289, 107615.
Zeng, S.B., Jiang, Y.J., Liu, Z.H., 2016. Assessment of climate impacts on the karst-related carbon sink in SW China using MPD and GIS. Glob. Planet. Chang. 144, 171–181.
Zhang, C., 2010. Seasonal variation of dissolution rate under the soil at different land uses and its influence factors a case study of Jinfo mountain, Chongqing. Geol. Rev. 56, 136–140.
Zhang, C., 2020. Moisture sources for precipitation in Southwest China in summer and the changes during the extreme droughts of 2006 and 2011. J. Hydrol. 591, 125333.
Zhang, E.L., Sun, W.W., Zhao, C., Wang, Y.B., Xue, B., Shen, J., 2015a. Linkages between climate, fire and vegetation in Southwest China during the last 18.5 ka based on a sedimentary record of black carbon and its isotopic composition. Palaeogeogr. Palaeoclimatol. Palaeoecol. 435, 86–94.
Zhang, H.L., Yu, K.F., Zhao, J.X., Feng, Y.X., Lin, Y.-S., Zhou, W., Liu, G.-H., 2013. East Asian Summer Monsoon variations in the past 12.5 ka, High-resolution $\delta^{18}O$ record from a precisely dated aragonite stalagmite in Central China. J. Asian Earth Sci. 73, 162–175.
Zhang, J., Liang, M.-Q., Li, T.-Y., Chen, C.-J., Li, J.-Y., 2022. Asian-Australian monsoon evolution over the last millennium linked to ENSO in composite stalagmite $\delta^{18}O$ records. Quat. Sci. Rev. 281, 107420.
Zhang, M., Yuan, D.-X., Lin, Y.-S., Qin, J.-M., Bin, L., Cheng, H., Edwards, R.L., 2004. A 6000-year high-resolution climatic record from a stalagmite in Xiangshui Cave, Guilin, China. The Holocene 14, 697–702.
Zhang, R.H., Sumi, A., Kimoto, M., 1996. Impact of El Niño on the East Asian monsoon. J. Meteorol. Soc. Jpn. Ser. II 74, 49–62.
Zhang, R.H., Min, Q.Y., Su, J.Z., 2017. Impact of El Niño on atmospheric circulations over East Asia and rainfall in China, role of the anomalous western North Pacific anticyclone. Sci. China Earth Sci. 60, 1124–1132.
Zhang, S.Y., Peng, F.R., 2012. On the song dynasty population migration to the national blend promote in the Wujiang River basin (in Chinese). Guizhou Ethnic Stud. 3, 122–127.
Zhang, X.G., 1980. Reform and construction of the Bozhou and the beginning and end of the Yang's. J. Guizhou 2, 23–28. Normal University (Social Sciences) (in Chinese).
Zhang, Y.Q., 2003. The transformation of the ethnic cultures in Guizhou during the North and South Song Dynasties (in Chinese). Guizhou Ethnic Stud. 1, 96–101.
Zhang, H.W., Cai, Y.J., Tan, L.C., Cheng, H., Qin, S.J., An, Z.S., Edwards, R.L., Ma, L., 2015b. Large variations of $\delta^{13}C$ values in stalagmites from southeastern China during historical times, implications for anthropogenic deforestation. Boreas 44, 511–525.
Zhang, Z., Leduc, G., Sachs, J.P., 2014. El Niño evolution during the Holocene revealed by a biomarker rain gauge in the Galápagos Islands. Earth Planet Sci. Lett. 404, 420–434.
Zhao, M., Li, H.-C., Shen, C.-C., Kang, S.-C., Chou, C.-Y., 2017. $\delta^{18}O$, $\delta^{13}C$, elemental content and depositional features of a stalagmite from Yelang Cave reflecting climate and vegetation changes since late Pleistocene in central Guizhou, China. Quat. Int. 452, 102–115.

Zhao, K., Wang, Y.J., Edwards, R.L., Cheng, H., Liu, D.B., Kong, X.G., 2015. A high-resolved record of the Asian summer monsoon from Dongge cave, China for the past 1200 years. Quat. Sci. Rev. 122, 250–257.

Zhao, K., Wang, Y.J., Edwards, R.L., Cheng, H., Liu, D.B., Kong, X.G., Ning, Y.F., 2016. Contribution of ENSO variability to the East Asian summer monsoon in the late Holocene. Palaeogeogr. Palaeoclimatol. Palaeoecol. 449, 510–519.

Zhu, Q.G., He, J.H., Wang, P.X., 1986. A study of circulation differences between East-Asian and Indian summer monsoons with their interaction. Adv. Atmos. Sci. 3, 466–477.